



# Microwave-responsive gadolinium metal-organic frameworks nanosystem for MRI-guided cancer thermotherapy and synergistic immunotherapy

Hao Cui<sup>a,1</sup>, Yu-Yue Zhao<sup>a,1</sup>, Qiong Wu<sup>c,1</sup>, Yan You<sup>f,1</sup>, Zhou Lan<sup>a</sup>, Ke-Long Zou<sup>a</sup>, Guo-Wang Cheng<sup>c</sup>, Hao Chen<sup>a</sup>, Yan-Hua Han<sup>c</sup>, Yan Chen<sup>a</sup>, Xiang-Dong Qi<sup>d,e,\*\*</sup>, Xian-Wei Meng<sup>c,\*\*\*</sup>, Li-Min Ma<sup>b,\*\*\*\*</sup>, Guang-Tao Yu<sup>a,\*</sup>

<sup>a</sup> Stomatological Hospital, School of Stomatology, Southern Medical University, Guangzhou, 510280, China

<sup>b</sup> Medical Research Center, Guangdong Provincial People's Hospital (Guangdong Academy of Medical Sciences), Southern Medical University, Guangzhou, 510080, China

<sup>c</sup> Laboratory of Controllable Preparation and Application of Nanomaterials, Technical Institute of Physics and Chemistry, Chinese Academy of Sciences, Beijing, 100190, China

<sup>d</sup> Science and Technology Innovation Center, Guangzhou University of Chinese Medicine, Guangzhou, 510405, China

<sup>e</sup> Department of Plastic Surgery, Zhujiang Hospital, Southern Medical University, Guangzhou, 510280, China

<sup>f</sup> Department of Endodontics, Southern Medical University-Shenzhen Stomatology Hospital (Pingshan), Shenzhen, 518118, China

## ARTICLE INFO

**Keywords:**  
Immunotherapy  
Microwave  
Metal-organic framework  
Thermotherapy  
Cancer imaging

## ABSTRACT

The clinical application of cancer immunotherapy is unsatisfied due to low response rates and systemic immune-related adverse events. Microwave hyperthermia can be used as a synergistic immunotherapy to amplify the antitumor effect. Herein, we designed a Gd-based metal-organic framework (Gd-MOF) nanosystem for MRI-guided thermotherapy and synergistic immunotherapy, which featured high performance in drug loading and tumor tissue penetration. The PD-1 inhibitor (aPD-1) was initially loaded in the porous Gd-MOF (Gd/M) nanosystem. Then, the phase change material (PCM) and the cancer cell membrane were further sequentially modified on the surface of Gd/MP to obtain Gd-MOF@aPD-1@CM (Gd/MPC). When entering the tumor microenvironment (TME), Gd/MPC induces immunogenic death of tumor cells through microwave thermal responsiveness, improves tumor suppressive immune microenvironment and further enhances anti-tumor ability of T cells by releasing aPD-1. Meanwhile, Gd/MPC can be used for contrast-enhanced MRI. Transcriptomics data revealed that the downregulation of MSK2 in cancer cells leads to the downregulation of c-fos and c-jun, and ultimately leads to the apoptosis of cancer cells after treatment. In general, Gd/MPC nanosystem not only solves the problem of system side effect, but also achieves the controlled drug release via PCM, providing a promising theranostic nanoplatform for development of cancer combination immunotherapy.

## 1. Introduction

Despite rapid medical advances in the last two decades, cancer

remains one of the most difficult diseases to cure and is the second leading cause of death in the world, according to the World Health Organization (WHO) in 2020 [1]. As an emerging and promising

Peer review under responsibility of KeAi Communications Co., Ltd.

\* Corresponding author. Stomatological Hospital, Southern Medical University, No 366, Jiangnan Road, Haizhu Region, Guangzhou, 510280, China.

\*\* Corresponding author. Department of Plastic Surgery, Zhujiang Hospital, Southern Medical University, No 253 Gongye Avenue, Haizhu District, Guangzhou City, 510280, China.

\*\*\* Corresponding author. Laboratory of Controllable Preparation and Application of Nanomaterials, Technical Institute of Physics and Chemistry, Chinese Academy of Sciences, No 52 Sanlihe Road, Xicheng District, Beijing City, 100190, China:

\*\*\*\* Corresponding author. Medical Research Center, Guangdong Provincial People's Hospital (Guangdong Academy of Medical Sciences), Southern Medical University, No. 106, Zhongshan 2nd Road, Yuexiu District, Guangzhou City, 510080, China:

E-mail addresses: [qixiangdong@smu.edu.cn](mailto:qixiangdong@smu.edu.cn) (X.-D. Qi), [mengxw@mail.ipc.ac.cn](mailto:mengxw@mail.ipc.ac.cn) (X.-W. Meng), [malimin@gdph.org.cn](mailto:malimin@gdph.org.cn) (L.-M. Ma), [guangtao1986@smu.edu.cn](mailto:guangtao1986@smu.edu.cn) (G.-T. Yu).

<sup>1</sup> These authors contributed equally to this work.

<https://doi.org/10.1016/j.bioactmat.2023.11.010>

Received 9 August 2023; Received in revised form 16 November 2023; Accepted 16 November 2023

2452-199X/© 2023 The Authors. Publishing services by Elsevier B.V. on behalf of KeAi Communications Co. Ltd. This is an open access article under the CC BY-NC-ND license (<http://creativecommons.org/licenses/by-nc-nd/4.0/>).

therapy, cancer immunotherapy has been approved in the clinical treatment of some cancer patients with the aim of unleashing the anti-tumor function of the patient's immune system [2,3]. However, low response rates and systemic immune-related adverse events lead to effective and durable responses to immunotherapy in only a small number of patients, which is mainly attributed to low tumor-specific T cell infiltration in the tumor microenvironment [4–7]. Hyperthermia, which involves raising the temperature to induce cell death through apoptosis or necrosis, has been shown to enhance anti-tumor efficacy in combination with immunotherapy [8,9]. However, the therapeutic effectiveness of hyperthermia can vary depending on a variety of factors such as treatment mode, temperature, duration of treatment exposure, and tissue characteristics [10,11]. Therefore, the appropriate way of hyperthermia and thermal sensitive agents are very important for hyperthermia.

Microwave has been extensively explored in biomedical application, which radiation on a scale of 300 MHz to 300 GHz [12,13]. Microwave thermal therapy (MWTT) is a promising treatment method for cancer

owing to its deep biological tissue penetration, with negligible attenuation and minimal damage to tumor-adjacent tissues and cells [14–17]. Moreover, existing studies have shown that tumor tissue and inflammation sites absorb microwaves more significantly compared to healthy tissue [18]. These characteristics make microwave thermal therapy more suitable for cancer therapy. However, given microwave sensitizers inability to wake up exhausted T cells and complex tumor microenvironment, the MWTT alone is not enough to clear tumor [19]. Therefore, MWTT combining with immunotherapy is a promising option for cancer treatment.

Generally, the microwave sensitizers are divided into categories, including inorganic agents and organic agents. As an organic-inorganic hybrid material, metal-organic framework (MOF) nanoparticles have the advantages of both inorganic and organic agents. MOF is a promising hybrid porous material composed of metal ions and organic linkers, which has been applied in gas storage, catalysis, drug delivery, etc. [15, 20–23]. And, the adjustable pore size and high specific surface area lead to the unique advantages of MOF materials in drug loading [24,25].

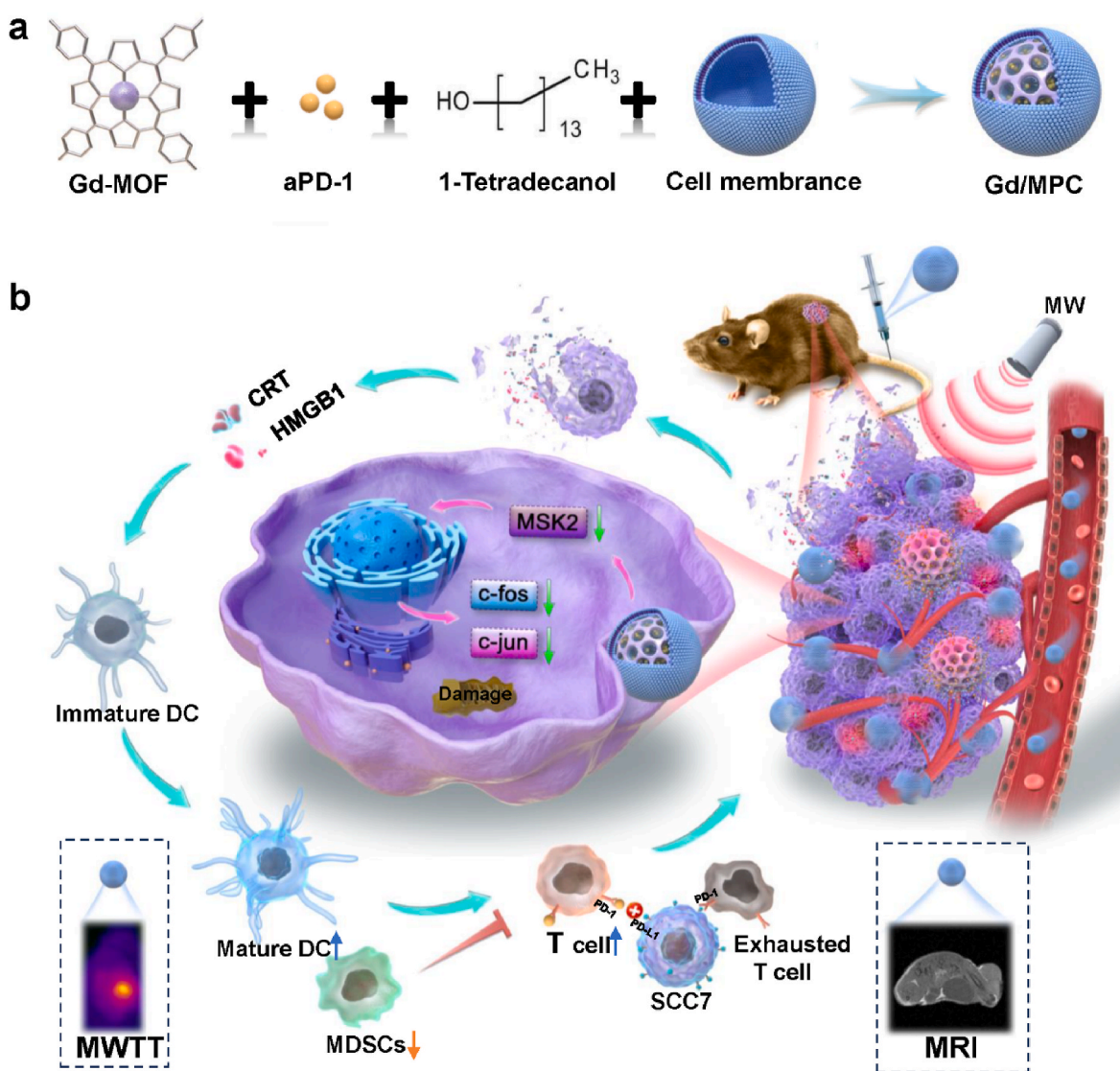


**Fig. 1.** Schematic illustration of the synthesis process and therapeutic effects of Gd-MOF@aPD-1@CM(Gd/MPC). a) Schematic diagram of the fabrication of Gd/MPC followed by Gd-MOF of loading anti-PD-1 (aPD-1) was sequentially packaged with 1-Tetradecanol and SCC7 membrane vesicles. b) Application of Gd/MPC for MRI-guided cancer combination therapy. First, SCC7 membrane vesicles modification augments the enrichment of Gd/MPC in tumor site. Then, microwave therapy was initiated after MRI revealed a high concentration of Gd/MPC in tumor microenvironment. The microwave thermal effect causes the solid-liquid transformation of 1-Tetradecanol to release aPD-1, which realized microwave thermal therapy-augmented cancer immunotherapy. Furthermore, the underlying molecular mechanism and changes of tumor immune microenvironment was presented, suggesting powerful tumor killing ability and anti-tumor immune response.

However, in vivo retention of MOF at tumor sites and uncontrollable drug release are major challenges for their biomedical applications [22, 25,26]. Therefore, a kind of conditionally responsive MOF materials need to be developed to overcome these weaknesses.

Nanomaterials as magnetic resonance imaging (MRI) contrast agents have great potential in improving the accuracy of cancer therapy [27]. Based Gd act as a kind of magnetic resonance imaging (MRI) contrast agent, Gd-derived nanoparticle was widely developed by researchers [28,29]. Herein, we constructed a cancer cell membrane coated Gd-MOF-loaded PD-1 inhibitor (Gd-MOF@aPD-1@CM, named Gd/MPC) nanocomposite as a microwave hyperthermia and MR imaging multifunctional nanoplatform for cancer therapy (Fig. 1). In brief, Gd-MOF was synthesized by solvothermal method. And then, PCM phase change materials (1-tetradecyl alcohol) were used for encapsulation after PD-1 inhibitor (aPD-1) loading into Gd-MOF, which improves the enrichment of drugs in tumors and the efficiency of microwave thermal

effects. Finally, the ability of homologous targeting was obtained through the SCC7 cell membrane embellish. As a result, the integration of MWTT and immune checkpoint inhibitor therapy of Gd/MPC would be achieved to efficiently cancer suppression in an MRI guiding and microwave-responsive manner. Furthermore, transcriptomic data and cytometry flow analysis revealed the regulation of molecular mechanism and changes of tumor immunosuppressive microenvironment after Gd/MPC treatment. Ours work opens up a new avenue for designing imaging-guided and stimulus-responsive nanosystem that can enhance cancer therapy.

## 2. Results and discussion

### 2.1. Fabrication and characterization of Gd/MPC

In general, the preparation of Gd/MPC includes the following parts:

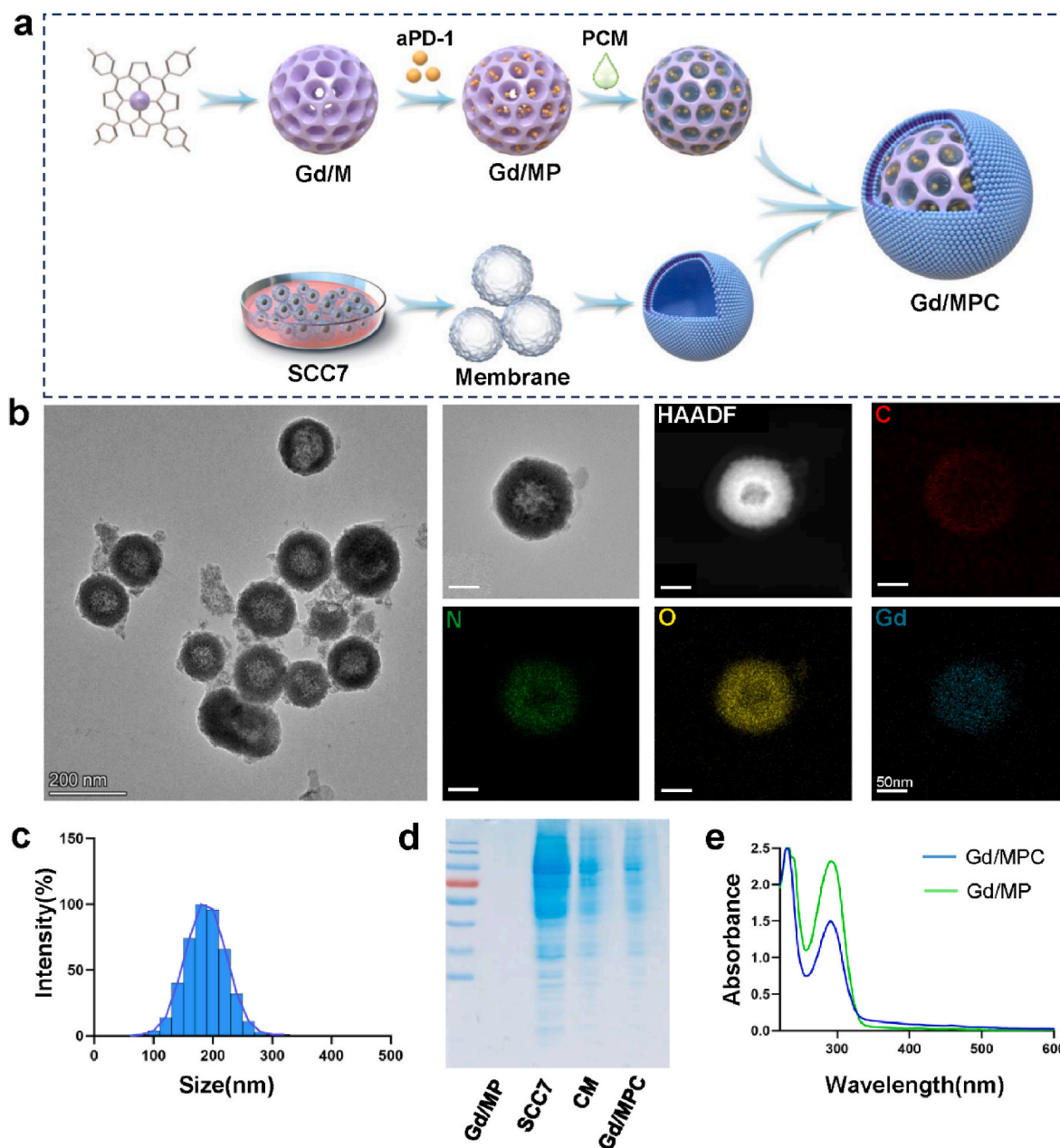


**Fig. 2.** Synthesis and characterization of Gd/MPC. a) Synthetic steps of Gd/MPC. b) TEM images and element mapping of Gd/MPC. c) Hydrodynamic size distribution of Gd/MPC. d) Coomassie bright blue stain of Gd/MP, SCC7 cells, CM and Gd/MPC. e) UV-vis-NIR spectra of Gd/MP and Gd/MPC.

1) Synthesis of Gd-MOF (Gd/M) materials by solution thermal synthesis. 2) Modification of aPD-1 into Gd/M material to obtain Gd-MOF@aPD-1 (Gd/MP). The XRD pattern of Gd/M and Gd/MP showed the successful modification of aPD-1 (Fig. S1a). In addition, the load aPD-1 was quantified by UV-vis-NIR spectra. The results showed that the proportion of aPD-1 in Gd/MP was about 28.23% (Figs. S1b–d). 3) 1-Tetradecanol is one of the most common PCM materials, with a melting point of about 38–40 °C (Figs. S2a–b). Compared with the same volume of water, the cooling efficiency of 1-Tetradecanol is slower than that of water at the same revelation temperature, and it can still remain above 33 °C (room temperature is 28 °C) after 5 min, which indicates that PCM materials release a certain amount of heat when the phase transition (Fig. S2c). Thermogravimetric analysis shows that the mass ratio of 1-Tetradecanol in Gd/MP is about 28% (Fig. S2d). SEM images show that Gd/M materials are more likely to agglomerate after modification of PCM (Fig. S2e). 4) Finally, SCC7 cells were cultured in vitro and the cell membrane was extracted, and then wrapped on the surface of Gd/MP to obtain Gd-MOF@aPD-1@CM (Gd/MPC) (Fig. 2a).

To ensure the successful preparation of Gd/MPC, the morphology of nanoparticles was characterized by TEM and elemental mapping. As shown in Fig. S3, Gd/MP is spherical with an average particle size of

about 163 nm (Fig. S4). After modification of the SCC7 cell membrane, the average particle size of Gd/MPC changed to 182 nm (Fig. 2c). The difference of nanoparticle size before and after the envelope is consistent with the reported cell membrane of 5–10 nm [30]. TEM further showed that Gd/MPC was surrounded by a film (Fig. 2b). And the main element distribution of Gd/MPC is C, N, O, Gd (Fig. 2b). Sodium dodecyl sulfate-polyacrylamide gel electrophoresis (SDS-PAGE) streaks show that membrane transfer of SCC7 does not affect the expression of membrane proteins in Gd/MPC (Fig. 2d).

The aqueous solutions of Gd/MPC with different concentrations were characterized by UV spectrophotometer. The results showed that the UV-Vis-NIR absorption peak of Gd/MP and Gd/MPC appeared at 292 nm, and the change of absorbance after coating SCC7 cell membrane was negligible (Fig. 2e). Studies have shown that in acidic media, water molecules attack metal oxide clusters in MOFs and degrade metal-organic bonds [31]. To simulate the acidic microenvironment of tumors, we placed the Gd/MP materials in PBS with pH 7.4 and 6.5, respectively. The release curve of aPD-1 showed that PBS solution with pH 6.5 was more likely to promote Gd/MP degradation, while microwave did not significantly promote Gd/MPC degradation. (Fig. S5).

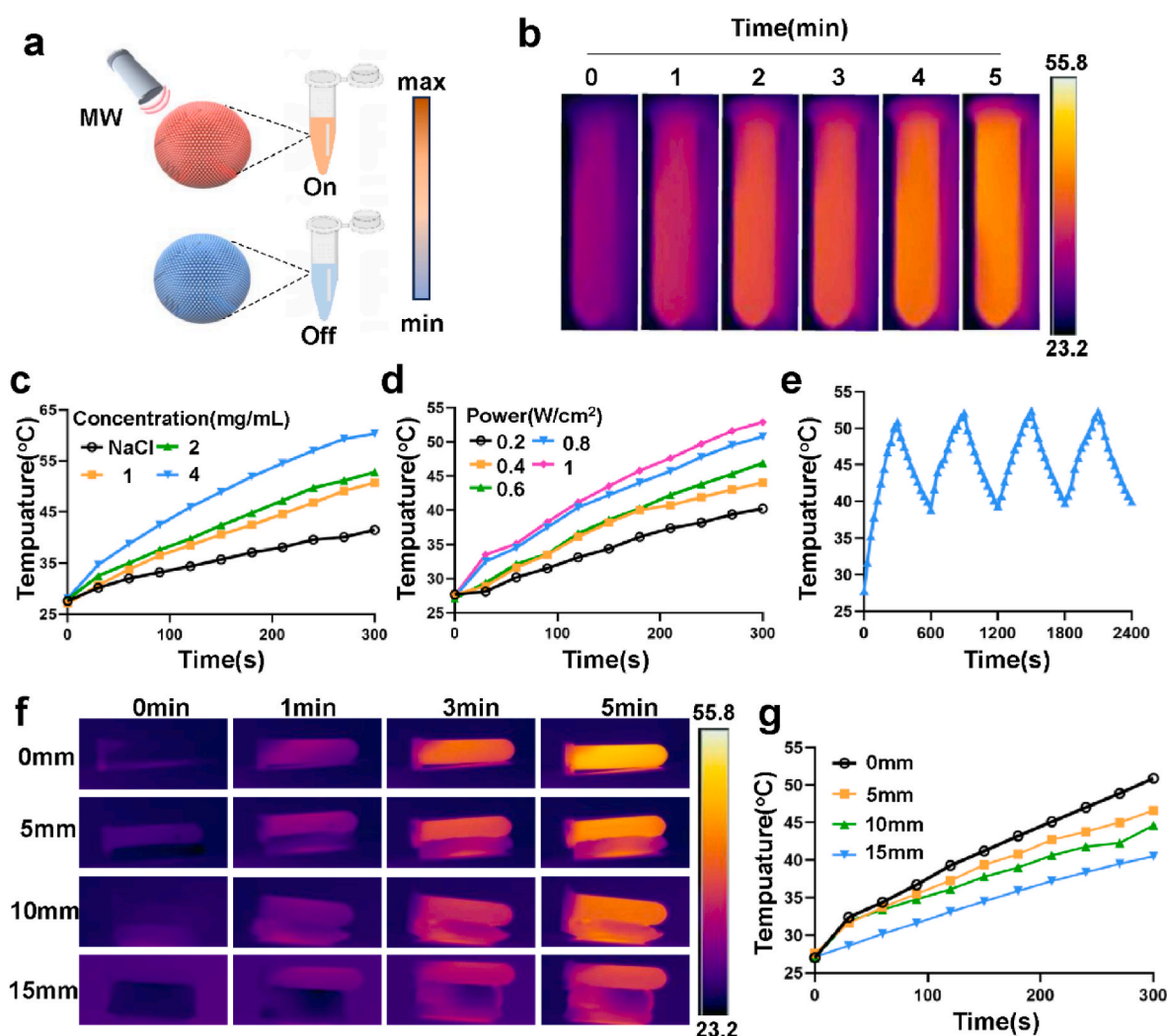


**Fig. 3.** Evaluation of microwave thermal effect. a) Schematic diagram of Gd/MPC microwave thermal effect. b) Microwave thermal images of Gd/MPC in different time points under microwave radiation (1 mg/mL, 0.6 W/cm<sup>2</sup>). c) The heating curve of Gd/MPC with different concentration (0, 1, 2, 4 mg/mL) under microwave radiation (0.6 W/cm<sup>2</sup>). d) The heating curve of Gd/MPC with different powers (0.2, 0.4, 0.6, 0.8, 1.0 W/cm<sup>2</sup>) under microwave radiation (1 mg/mL). e) The heating curve of Gd/MPC under microwave radiation (1 mg/mL, 0.6 W/cm<sup>2</sup>). f) Microwave thermal images of Gd/MPC under microwave radiation on pork tissues of different thicknesses (0, 5, 10, 15 mm, 1 mg/mL, 0.6 W/cm<sup>2</sup>). g) The heating curve of Gd/MPC under microwave radiation on pork tissues of different thicknesses (0, 5, 10, 15 mm, 1 mg/mL, 0.6 W/cm<sup>2</sup>).

## 2.2. The microwave thermal property of Gd/MPC

Abundant electronic energy levels and a large number of energy level transitions in electronic configurations make lanthanide europium metal-organic frameworks the most potential microwave sensitizers [32, 33]. To investigate the microwave thermal effect of Gd/MPC, H<sub>2</sub>O and a

series of concentrations of Gd/MPC were irradiated under microwave irradiation at 0.6 W/cm<sup>2</sup> for 5 min (Fig. 3a–b). The results showed that with the increase of the concentration of Gd/MPC, the heating curve of the solution showed concentration dependence (Fig. 3c). And when the concentration of Gd/MPC was 1 mg/mL, the temperature of the solution continued to increase within 5 min and exceeded 45 °C, which was

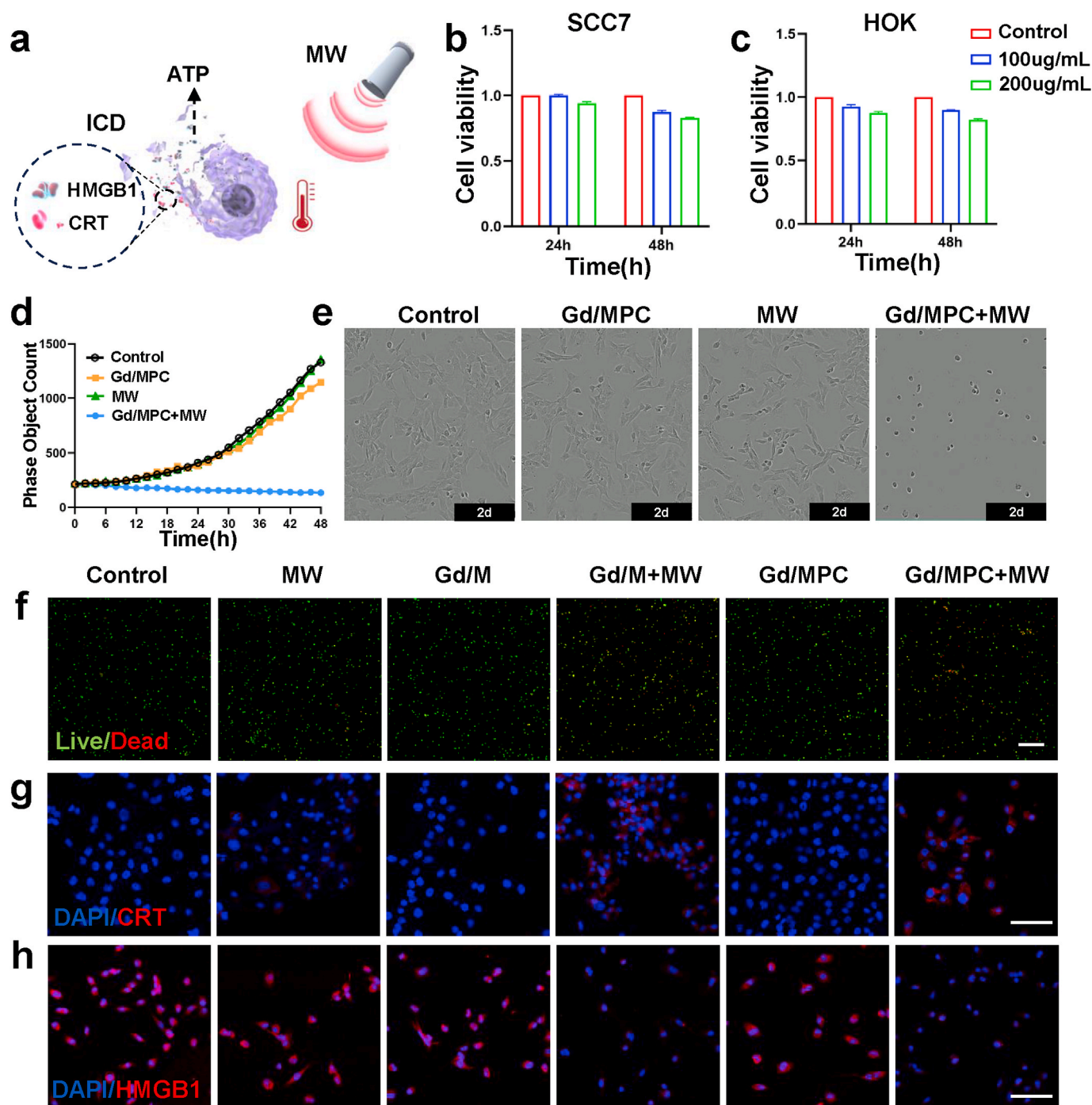


**Fig. 4.** The evaluation of ICD effects in vitro. a) Schematic diagram of ICD effect of tumor cells caused by microwave thermal effects. b) The SCC7 cell viability with different concentration Gd/MPC co-incubation (100, 200  $\mu$ g/mL) in different treatment time. c) The HOK cell viability with different concentration Gd/MPC co-incubation (100, 200  $\mu$ g/mL) in different treatment time,  $n = 3$ . d) Proliferation curves of SCC7 cells under different treatments (control, Gd/MPC 100  $\mu$ g/mL, MW 0.6W/cm<sup>2</sup>, Gd/MPC + MW). e) Images of SCC7 cells at 48 h after different treatments (control, Gd/MPC 100  $\mu$ g/mL, MW 0.6W/cm<sup>2</sup>, Gd/MPC + MW). f) Immunofluorescence images of live/dead staining of SCC7 cells with or without nanoparticles (Gd/M or Gd/MPC, 100  $\mu$ g/mL) co-incubation under microwave radiation treatment (0.6 W/cm<sup>2</sup>, 5 min). Scale bar: 400  $\mu$ m. g) Immunofluorescence images of CRT expression on SCC7 cells with or without nanoparticles (Gd/M or Gd/MPC, 100  $\mu$ g/mL) co-incubation under microwave radiation treatment (0.6 W/cm<sup>2</sup>, 5 min). Scale bar: 100  $\mu$ m. h) Immunofluorescence images of HMGB1 expression on SCC7 cells with or without nanoparticles (Gd/M or Gd/MPC, 100  $\mu$ g/mL) co-incubation under microwave radiation treatment (0.6 W/cm<sup>2</sup>, 5 min). Scale bar: 100  $\mu$ m.

enough to induce immunogenic death of tumor cells. Similarly, at a fixed concentration of 1 mg/mL, as the microwave power increases, the heating curve of the solution also shows power dependence (Fig. 3d). Subsequently, the stability of Gd/MPC was verified in four switching cycles of microwave (1 mg/mL, 0.6W/cm<sup>2</sup>). It was found that the temperature of the Gd/MPC solution can still be kept above 40 °C after the microwave radiation is turned off, which may be related to the heat energy released when the PCM material undergoes morphological transformation. And after 4 cycles, Gd/MPC still showed a certain stability, indicating that the material can maintain good thermal stability only under microwave treatment (Fig. 3e). Finally, in order to simulate the penetration ability of microwaves to human tissue, the Gd-MOF material was placed on pork with different thicknesses. The results show that when the thickness exceeds 15 mm, microwave radiation can still promote the heating of Gd/MPC solution (Fig. 3f–g). These results indicate that Gd/MPC is an excellent microwave thermosensitive material.

### 2.3. Gd/MPC can effectively induce immunogenic cell death (ICD) of cancer cells

In vitro experiments, we first verified the uptake mechanism of SCC7 cells against Gd/MPC by introducing three uptake inhibitors [34]. The results showed that all three groups of inhibitors inhibited the phagocytosis of SCC7 cells, and the inhibition effect of fassa protein-mediated endocytosis was the most obvious (Fig. S6). Then we co-incubated Gd/MP<sup>Cy5</sup> and Gd/MPC<sup>Cy5</sup> with SCC7 cells respectively, and the results showed that more fluorescence was expressed in the Gd/MPC group, indicating that Gd/MPC was more easily taken up by SCC7 cells (Fig. S7). The occurrence of ICD in tumor cells caused by thermal effects is often the most important auxiliary method for tumor immunotherapy [35]. Analogically, the microwave thermoresponsive ability of Gd/MPC should be able to induce the ICD of tumor cell (Fig. 4a). In order to verify this phenomenon, firstly, the cell killing effect of the Gd/MPC itself was explored. aPD-1 plays an indirect role in tumor inhibition by activating disabled T cells, and cannot inhibit tumor cells by themselves under in vitro cell culture conditions (without the presence of immune cells). Different concentrations of Gd/MPC were added to the medium of SCC7 cells and HOK cells for co-incubation. After 48 h, CCK8 detection results showed that Gd/MPC had no significant effect on the proliferation of SCC7 cells or HOK cells (Fig. 4b–c). Then, in order to verify the microwave thermal effect of Gd/MPC on SCC7 cells, cell proliferation was analyzed by live cell workstation under different treatments (Control group, MW group, Gd/MPC group Gd/MPC + MW) (Fig. 4d–e). The results showed that under the influence of MW, the medium only reached 40 °C at 5 min, and the proliferation of SCC7 was not affected (Figs. S8–S10). On the contrary, the medium temperature of the Gd/MPC group was close to 50 °C, and the SCC7 cells basically did not proliferate within 48 h (Figs. S8–S10). This indicated that the microwave thermal effect of Gd/MPC could effectively inhibit the viability of SCC7 cells.

Accumulative studies have shown that thermal effects can cause the ICD effect of tumor cells and ICD has become a bridge for the interaction of tumor cell microenvironment by enhancing the immunogenicity of tumor cells [36,37]. ICD emergence stimulates damage-associated molecular patterns leading to release of HMGB1, CRT and ATP to promote antitumor immunity [38]. In order to prove whether Gd/MPC can induce ICD under microwave irradiation, we analyzed the expression of HMGB1 and CRT of SCC7 cells under different treatments by immunofluorescence. Confocal results showed that cells in Gd/M + MW and Gd/MPC + MW groups died obviously (Fig. 4f). Correspondingly, the expression of CRT in the cytoplasm was increased and the expression of HMGB1 in the nucleus was decreased (Fig. 4g–h). Subsequently, we detected the supernatant in each group of cells, and the results showed that the content of ATP in the supernatant of Gd/MP + MW and Gd/MPC + MW groups increased significantly and ATP also significantly

increased (Fig. S11). The above results indicated that microwave thermal effect induced ICD in SCC7 cells. Since aPD-1 does not cause the death of SCC7 cells in vitro, in order to determine the specific cell death mode in this process, we stained different groups of cells (control, Gd/MPC, Gd/MPC + MW) through Hoechst33342 and PI double staining methods. The results showed that more apoptosis occurred in Gd/MPC + MW group (Fig. S12). These results suggest that Gd/MPC is a promising tumor immunotherapeutic agent.

### 2.4. Multimodal imaging of Gd/MPC

Cancer cell membranes can express tumor surface related proteins such as CD44 to incubate the immune escape of nanomaterials, combined with the homologous targeting ability of cancer cell membranes, which is conducive to more drug enrichment in tumors and enhance the anti-tumor effect of drugs [39–41]. To validate the role of SCC7 cell membranes play in drug delivery system, we modified Cy5 fluorescent dye onto Gd/MP to obtain Gd/MP<sup>Cy5</sup>, and then injected Gd/MP<sup>Cy5</sup> and Gd/MP<sup>Cy5</sup> into C3H tumor-bearing mice via caudal vein, respectively, and observed the expression of fluorescence signals in tumors within 24 h (Fig. 5a). The results showed that the fluorescence signal of Cy5 reached the highest within 4 h, and then decreased slowly. It was found that the expression of fluorescence signal of Gd/MP<sup>Cy5</sup> in tumor was higher than that of Gd/MP<sup>Cy5</sup> through fluorescence quantification (Fig. 5b–c). This suggests that cancer cell membranes increase Gd/MPC accumulation in tumors, suggesting the function of reducing the toxicity and increasing effect of Gd/MPC.

Gadolinium has unique magnetic properties and important diagnostic applications in MR Imaging [28,42]. So, we tested the MRI ability of Gd/MPC subsequently. After Gd/MPC was administered to tumor-bearing mice at different times, the distribution of Gd<sup>3+</sup> in different tissues was detected by ICP. The results showed that Gd<sup>3+</sup> reached its highest value within 4h of the tumor, which is the same as the results of in vivo fluorescence imaging. In addition, within 24h, the element content of the lungs gradually decreased while that of the liver and spleen gradually increased, indicating that Gd<sup>3+</sup> is mainly metabolized by the liver (Fig. S13). In vitro, the T1-weighted MR signal of Gd/MPC solution showed a concentration-dependent effect (Fig. 5d–e and Fig. S14). Gd/MPCs were then injected into C3H tumor-bearing mice through the tail vein (Fig. 5a). As with the results of fluorescence imaging, the MR signal of the whole mouse was also enhanced at 4h. And after 24h, the MR intensity of tumor tissue was significantly higher than that before treatment (Fig. 5f–g). This indicates that Gd/MPC can safely circulate and accumulate in tumor tissues, and it can be used as a good contrast agent in tumor MR imaging.

### 2.5. In vivo antitumor immunotherapy efficacy of Gd/MPC

To evaluate the immunotherapeutic effect of Gd/MPC, a tumor inhibition assay was performed in a C3H tumor-bearing mouse model (Fig. S15a). In order to reduce the effect of microwave thermal effects on normal tissues, we select a working probe that matches the size of the tumor tissue for treatment (Fig. S15b). Thirty-five C3H mice were randomly divided into 7 groups as follows: G1: PBS, G2: Gd/M, G3: PBS + MW, G4: Gd/M + MW, G5: aPD-1, G6: Gd/MP, G7: Gd/MPC + MW. Then 1 × 10<sup>6</sup> SCC7 cells were inoculated into the back of C3H mice. When the tumor grew for about 5 days and the average tumor volume reached 50 mm<sup>3</sup>, the corresponding treatment was started on the mice. Four hours after intravenous injection, the tumor site was treated with microwave (0.6W/cm<sup>2</sup>) for 10 min continuously (Fig. 6a). Representative thermal imaging images from G3, G4, and G7 mice are shown in Fig. 6b. Due to the rich blood vessels in the tumor tissue, combined with the characteristics of microwave heating, the tumor tissue can reach close to 50 °C in 10 min under simple microwave radiation. But in the G4 and G7 groups, the temperature inside the tumor tissue was close to 55 °C, which indicated that the drug was enriched in the tumor (Fig. 6c).

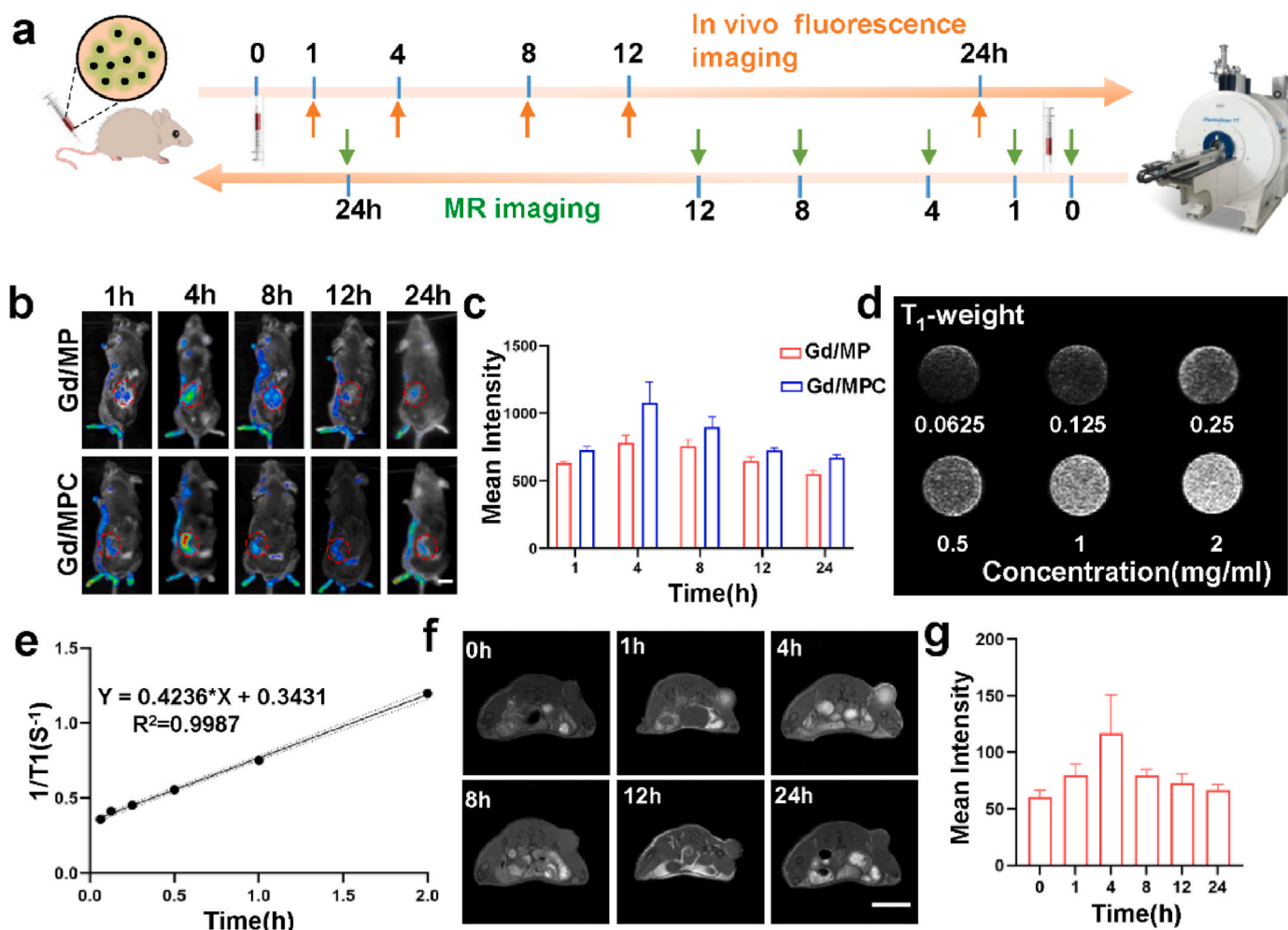
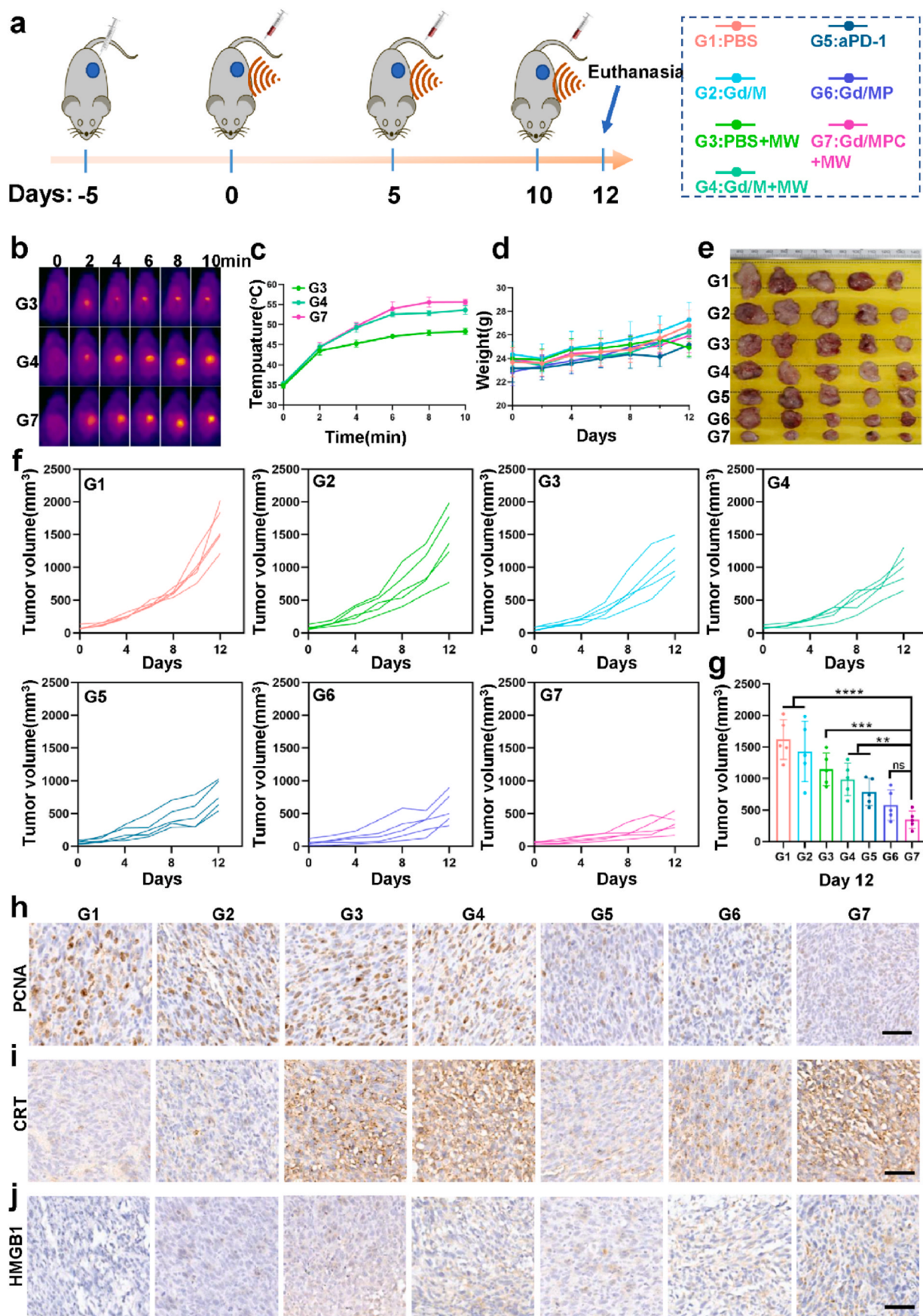


**Fig. 5.** The multimodal imaging of Gd/MPC. a) Research design of in vivo fluorescence imaging and MR Imaging ability of C3H mice. b) The enrichment of fluorescent signals in tumors of C3H mice treated with Gd/MP and Gd/MPC at different times. Scale bar:1 cm. c) Quantitative mean fluorescence intensities of tumors in different groups at various time points ( $n = 3$ ). d) T<sub>1</sub>-weight MRI images of Gd/MPC at different concentration. e) Linear curve of relaxation rate ( $1/T_1$ ) versus the Gd/MPC concentration. f) In vivo T<sub>1</sub>-weighted MR images of tumor bearing-C3H mice before and after intravenous injection of Gd/MPC. Scale bar:1 cm. g) Quantitative mean MR intensities of tumors at various time points ( $n = 3$ ).

Routinely, the body weight and tumor volume of the mice were monitored every two days. During treatment, the changes of body weight in Gd/MPC + MW treatment group were comparable to the rest of the group, indicating Gd/MPC with a low risk of serious side effects (Fig. 6d). The photographs and curve of tumor growth showed that the G1 (PBS) group had a rapid increase in tumor volume, and G2 (Gd/M) group had no obvious inhibitory effect on the tumor. Due to the thermal effect of microwave, the tumor volume of G3(PBS + MW) group and G4 (Gd/M + MW) group was smaller than that of PBS group. Compared with the therapeutic effect of aPD-1treatment (G5) group on C3H mice, the therapeutic effect of G6 (Gd/MP) group was better, mainly due to the more enrichment of the drug in vivo. Besides, the G7(Gd/MPC + MW) group showed the most excellent anti-tumor effect due to hyperthermia combined with ICB therapy (Fig. 6 e-g and Fig. S16). The tumors of C3H were collected at 12 days for flow analysis, immunohistochemistry, immunofluorescence and Western blot. The results showed that the staining of PCNA in the G7 group was weak, indicating that G7 treatment successfully weakened the proliferative ability of cancer cells (Fig. 6h). However, the expression of immunohistochemical staining of HMGB1 and CRT increased in the G3, G4 and G7 groups, indicating that the microwave thermal effect exerts anti-tumor immune function through CRT in vivo (Fig. 6i–j). IFN- $\gamma$  is a soluble dimer factor, most of which is secreted by activated natural killer cells NK and natural killer T

cells (NKT), and its main biological functions are anti-tumor, antiviral and immune regulation [43]. We found that IFN- $\gamma$  showed high expression in G7 group by immunohistochemical staining, which indicated that the combination of microwave hyperthermia and aPD-1 had the most significant changes in the tumor microenvironment (Fig. S17). In order to evaluate the anti-tumor effects of different components of the entire nanomaterial therapy system, we compared the tumor volume changes between different groups. Comparing the tumor volume of the G6 (Gd/MP) and G5 (aPD-1) groups showed that the MOF nanomedical drug delivery system improved the anti-tumor effect by approximately 26%. Comparing the tumor volume of G2 (Gd/M) and G3 (Gd/M + MW) groups showed that the microwave thermal effect increased the anti-tumor effect by 15%. A comparison of tumor volume between G2 (Gd/M) and G6 (Gd/MP) showed that the presence of aPD-1 increased the antitumor effect by 59%. By comparing the tumor volume of Gd/MP group and Gd/MPC group, the homologous cell membrane increased the anti-tumor ability by 15% (Fig. S18). The above results show that in the drug system, aPD-1 as the core drug exerts the greatest anti-tumor effect, while the nano delivery system, microwave and release membrane all enhance the ultimate anti-tumor effect.

PD-1 blocking therapy is to exert the tumor-killing ability of T cells by blocking the binding process of PD-1 receptors on the surface of T cells and PD-L1 on the surface of tumor cells [44–46]. To confirm the



(caption on next page)

**Fig. 6.** In vivo microwave thermotherapy and immunotherapeutic efficacies of Gd/MPC on SCC7 tumor-bearing C3H mice. a) Construction of C3H tumor model and design of treatment plan. b) Representative thermographic images from mice under a microwave radiation treatment ( $0.6 \text{ W/cm}^2$ ) at 4 h post i.v. injection of PBS, Gd/M and Gd/MPC. c) The curve of temperature of tumor site in different groups at various time points. d) The weight growth curves of different groups of mice. e) Tumor images in vitro of different groups of mice ( $n = 5$ ). f) The curve of tumor growth in different treatment groups (Microwave radiation was conducted at 4 h post-injection nanoparticles for consecutive 10 min,  $0.6 \text{ W/cm}^2$ ,  $n = 5$ ). g) Tumor volume on day 12 in different group (Two-way ANOVA with Sidak's multiple comparisons test, ns: no significance, \*\*:  $p < 0.01$ , \*\*\*:  $p < 0.001$ , \*\*\*\*:  $p < 0.0001$ ,  $n = 5$ ). h) The PCNA immunohistochemical staining images of tumor biopsies from different treatment groups. Scale bar:  $50 \mu\text{m}$ . i) The CRT immunohistochemical staining images of tumor biopsies from different treatment groups. Scale bar:  $50 \mu\text{m}$ . j) The HMGB1 immunohistochemical staining images of tumor biopsies from different treatment groups. Scale bar:  $50 \mu\text{m}$ .

regulation of tumor immune microenvironment by Gd/MPC combined with microwave thermal therapy, we analyzed the changes of immune cell populations in tumors using flow cytometry. The gating strategy for flow cytometry is shown in Fig. 7a. Dendritic cells (DCs), as the most important antigen-presenting cells, play a vital role in T cell activation by presenting antigens to T cell receptors [47]. And  $\text{CD103}^+$  DCs are the only APCs that deliver intact antigen to lymph nodes and prime tumor-specific  $\text{CD8}^+$  T cells [48].  $\text{CD103}^+$  DCs are required to promote antitumor effects upon checkpoint ligand PD-L1 blockade. Here, compared with other groups, the number of  $\text{CD11b}^+\text{CD11c}^+$ DCs and  $\text{CD103}^+$ DCs in the Gd/MPC + MW (G7) group was significantly increased, which may be related to the CRT and HMGB1 from ICD to promote the maturation of DC (Fig. 7b–c, S19a–b). MDSCs are major negative immune regulators that secrete cytokines for the exposure of effector T cells. After aPD-1 and microwave treatment, except for the G2 group, the number of MDSCs ( $\text{CD11b}^+\text{Gr-1}^+$ ) in the tumor microenvironment of other groups was significantly down-regulated, which is more conducive to the anti-tumor effect of T cells (Fig. 7d and Fig. S19c). With the decrease of MDSCs and the increase of DC, the number of  $\text{CD4}^+$  and  $\text{CD8}^+$  T cells in the Gd/MPC group also increased significantly (Fig. 7e–f, S19d–e). Finally, we analyzed the expression of PD-1 on  $\text{CD8}^+$  T cells in the tumor microenvironment of each group, and the results showed that the expression of PD-1 in the G2–G4 group decreased compared with the G1 group, but the difference was not statistically significant with the introduction of aPD-1 treatment, the expression of PD-1 in G5–G7 group was decreased (Fig. 7g, Fig. S19f). The above results show that Gd/MPC combined with microwave hyperthermia can effectively improve the immunosuppressive effect of tumor microenvironment on T cells.

## 2.6. Gd/MPC induces tumor cell apoptosis through MAPK signaling pathway

Subsequently, we explored the underlying biological mechanism of Gd/MPC for tumor inhibition by tumor specimen RNA sequencing from the G1 and G7 groups. The results showed that 11,801 were co-expressed in the G1 and G7 groups (Fig. 8a). The volcano plot showed that 148 genes were up-regulated and 468 genes were down-regulated after Gd/MPC + MW treatment (Fig. 8b). To gain further insight into the potential targeting pathways of Gd/MPC + MW, we performed Gene Ontology (GO) analysis (Fig. 8c and Fig. S20). The results show that positive regulation of cell activation, adaptive immune response and positive regulation of leukocyte activation (red arrows) are highly enriched. Finally, KEGG was used to analyze pathway changes in the tumor microenvironment before and after treatment. It was found that MAPK correlation pathway was significantly down-regulated after Gd/MPC + MW (Fig. 8d and Fig. S21). In down-regulated MAPK-related pathways, we found down-regulated expressions of MSK-2, C-Jun and C-Fos. Study shows MSK-2 can activate the proto-oncogenes c-jun and c-fos through mitosis in tumor cells [49]. And the expressions of c-jun and c-fos were related to apoptosis [50]. To verify this change of pathway, we found that the expressions of MSK, C-Jun and C-Fos proteins in G7 group were down-regulated compared with G1 group by Western blot (Fig. 8e). And immunohistochemical results showed that the expression of caspase3 was up-regulated in G7 group (Fig. S22). These results indicated that Gd/MPC + MW induced apoptosis of tumor cells through MAPK pathway. In order to verify whether the changes in pathways

would have the same trend in vitro, we re-grouped SCC7 cells accordingly. WB results showed that Gd/MPC had little effect on the proteins of MSK2, C-Fos and C-jun, while a slight trend was seen for Gd/MPC + MW. These results indicate that changes in the MAPK signaling pathway may be caused by the microwave thermal effect combined with the ICB effect rather than by a single pathway (Fig. S23).

## 2.7. Gd/MPC biosafety evaluation in vivo

On the basis of the original treatment plan, we injected Gd/MPC into the tail vein of ICR mice every 5 days to determine the biological safety of Gd/MPC. During the 24-day treatment, we performed body weight monitoring for ICR hours every two days. Result shows that there was no significant difference in body weight between the two groups of mice (Fig. S24). Subsequently, we collected peripheral blood from ICR mice on day 24 for complete blood count and blood biochemical analysis. We also collected the hearts, livers, spleens, lungs and kidneys of mice for histopathological (HE) analysis. The results showed no obvious abnormalities in hematology and biochemical results (Figs. S25–26). HE staining showed no obvious pathological changes in organs (Fig. S27). Since the metabolism of contrast agents in the body is intuitively important for clinical applications, we injected Gd/MPC into normal mice through the tail vein. The hearts, livers, spleens, lungs, kidneys, blood and feces of mice were collected for  $\text{Gd}^{3+}$  detection. The results showed that  $\text{Gd}^{3+}$  was more distributed in the liver, spleen and lungs, and less in the blood and feces (Fig. S28). These results indicated that Gd/MPC had good biosafety.

## 3. Conclusion

In this study, we successfully constructed a Gd-MOF@aPD-1 drug system (Gd/MPC) for cancer MRI-guided MWTT and immunotherapy. Gd/MPCs demonstrate superior immune evasion and active TME targeting properties, which depend on a cognate cancer cell membrane coating. As the core of drug carrier, Gd-based materials have excellent MRI imaging ability. The microwave thermal responsiveness of Gd-MOF can induce ICD of tumor cells, which can further enhance the anti-tumor immune response through CRT and HMGB1, and promote the maturation and antigen presentation of DC cells. Finally, Gd/MPC is gradually degraded in the acidic tumor microenvironment, releasing aPD-1, achieving a good tumor killing effect under the dual effects of ICD and aPD-1. In summary, our study constructs a multifunctional drug system Gd/MPC for multimodal cancer imaging and microwave immunotherapy. In the future, we believe that the Gd-MOF drug system will provide wider clinical transformation and application.

## Ethics approval and consent to participate

I confirm that I have obtained all consents required by applicable law for the publication of any personal details or images of patients, research subjects or other individuals that are used in the materials submitted to KeAi. I have retained a written copy of all such consents and I agree to provide KeAi with copies of the consents or evidence that such consents have been obtained if requested by KeAi.

Mice were fed in a suitable environment with food and water at  $22 \text{ }^\circ\text{C}$  and 41% humidity in a 12 h light/12 h dark cycle. All animal experiments were approved by the Ethics Committee of Guangdong Provincial

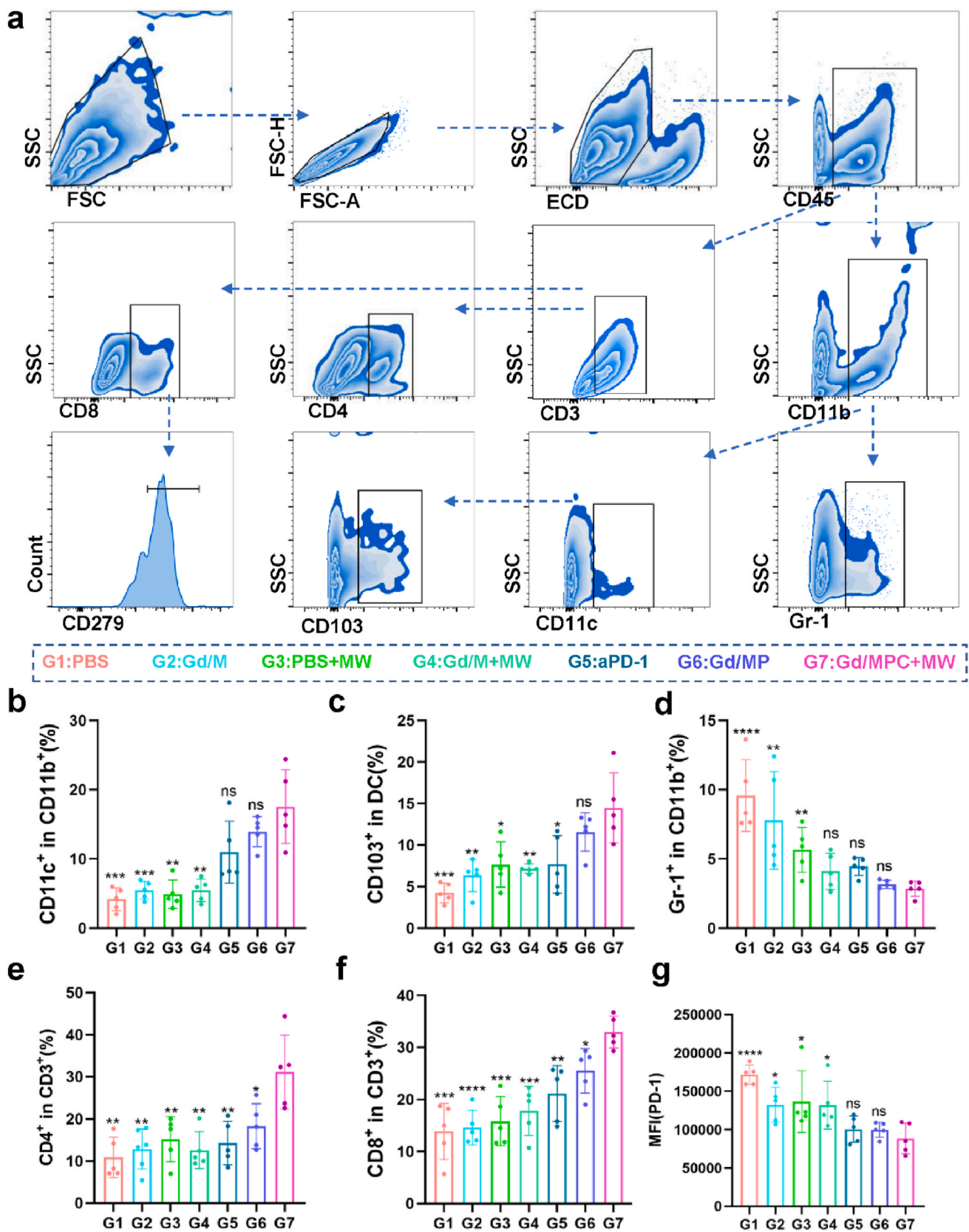
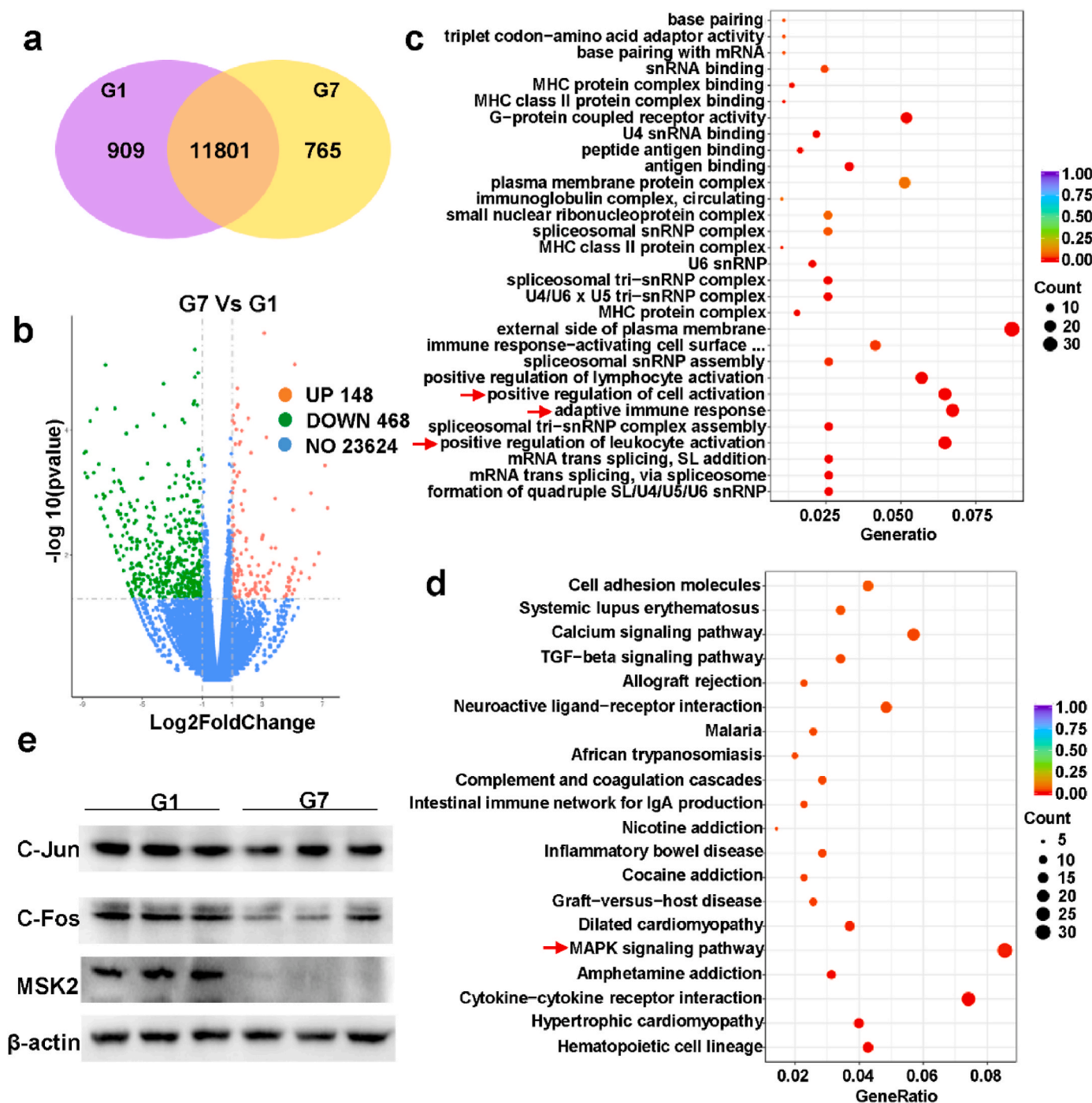


Fig. 7. The tumor immune microenvironment after different treatment. a) Flow gating strategy of immune cell population in tumor microenvironment of C3H tumor-bearing mice. b) Flow cytometric quantification of (b) dendritic cells (CD11b<sup>+</sup>CD11c<sup>+</sup>), (c) CD103<sup>+</sup> DC cells, (d) MDSCs (CD11b<sup>+</sup>Gr-1<sup>+</sup>), (e) CD4<sup>+</sup>T cells, (f) CD8<sup>+</sup> T cells, (g) PD-1(CD279) (Compared with G7, Ordinary one-way ANOVA with Dunnett's multiple comparisons test; ns: no significance, \*: p < 0.05, \*\*: p < 0.01, \*\*\*: p < 0.001, \*\*\*\*: p < 0.0001, n = 5).



**Fig. 8.** The biological mechanism of Gd/MPC by RNA sequencing. a) The venn map of G7(Gd/MPC + MW) and G1(PBS) group. b) The volcano map of G7(Gd/MPC + MW) and G1(PBS) group. c) Gene ontology enriched in G7 and G1 group (red arrow represent Gd/MPC relative pathways. d) Kyoto Encyclopedia of Genes and Genomes enriched in G7 and G1 group (red arrow represent Gd/MPC relative pathways. e) The western blotting of MAPK pathway (MSK2, C-Fos, C-Jun) in G1 and G7 group.

People’s Hospital (KY2023-054-01).

**CRedit authorship contribution statement**

**Hao Cui:** Writing – original draft, Methodology, Investigation, Conceptualization. **Yu-Yue Zhao:** Writing – original draft, Supervision, Funding acquisition. **Qiong Wu:** Writing – original draft, Project administration, Methodology. **Yan You:** Supervision, Formal analysis, Data curation. **Zhou Lan:** Software, Formal analysis. **Ke-Long Zou:** Formal analysis, Data curation. **Guo-Wang Cheng:** Validation,

Supervision. **Hao Chen:** Resources, Methodology. **Yan-Hua Han:** Validation. **Yan Chen:** Data curation. **Xiang-Dong Qi:** Writing – review & editing, Supervision, Formal analysis. **Xian-Wei Meng:** Visualization, Supervision, Methodology. **Li-Min Ma:** Writing – review & editing, Resources, Funding acquisition. **Guang-Tao Yu:** Writing – review & editing, Validation, Funding acquisition, Data curation, Conceptualization.

## Declaration of competing interest

The authors declare no conflict of interest.

## Acknowledgements

We thank financial support from National Natural Science Foundation of China [82103404], Southern Medical University Excellent Youth Scholars Training Program [2020YQPY008], Stomatological Hospital of Southern Medical University Startup Funds [No.PY2020001, PY2019026], Natural Science Foundation of Guangdong Province (2023A1515011604), The Fundamental Research Funds for the Central Universities (2022ZYGXZR042) and the High-level Hospital Construction Project (KJ012019100) for financial support.

## Appendix A. Supplementary data

Supplementary data to this article can be found online at <https://doi.org/10.1016/j.bioactmat.2023.11.010>.

## References

- [1] H. Sung, J. Ferlay, R.L. Siegel, M. Laversanne, I. Soerjomataram, A. Jemal, F. Bray, Global cancer statistics 2020: GLOBOCAN estimates of incidence and mortality worldwide for 36 cancers in 185 countries, *Ca - Cancer J. Clin.* (71) (2021) 209–249.
- [2] Y. Zhang, Z. Zhang, The history and advances in cancer immunotherapy: understanding the characteristics of tumor-infiltrating immune cells and their therapeutic implications, *Cell. Mol. Immunol.* 17 (2020) 807–821.
- [3] C. Pan, H. Liu, E. Robins, W. Song, D. Liu, Z. Li, L. Zheng, Next-generation immunology agents: current momentum shifts in cancer immunotherapy, *J. Hematol. Oncol.* 13 (2020) 29.
- [4] R. Nadal, A. Amin, D.M. Geynisman, M.H. Voss, M. Weinstock, J. Doyle, Z. Zhang, A. Viudez, E.R. Plimack, D.F. McDermott, R. Motzer, B. Rini, H.J. Hammers, Safety and clinical activity of vascular endothelial growth factor receptor (VEGFR)-tyrosine kinase inhibitors after programmed cell death 1 inhibitor treatment in patients with metastatic clear cell renal cell carcinoma, *Ann. Oncol.* (27) (2016) 1304–1311.
- [5] T. Kurino, R. Matsuda, A. Terui, H. Suzuki, T. Kokubo, T. Uehara, Y. Arano, A. Hisaka, H. Hatakeyama, Poor outcome with anti-programmed death-ligand 1 (PD-L1) antibody due to poor pharmacokinetic properties in PD-1/PD-L1 blockade-sensitive mouse models, *J. Immunother. Cancer* (8) (2020).
- [6] K.B. Pointer, S.P. Pitroda, R.R. Weichselbaum, Radiotherapy and immunotherapy: open questions and future strategies, *Trends Cancer* (8) (2022) 9–20.
- [7] L. Zhu, J. Liu, J. Chen, Q. Zhou, The developing landscape of combinatorial therapies of immune checkpoint blockade with DNA damage repair inhibitors for the treatment of breast and ovarian cancers, *J. Hematol. Oncol.* 14 (2021) 206.
- [8] H. Gavilán, S.K. Avugadda, T. Fernández-Cabada, N. Soni, M. Cassani, B.T. Mai, R. Chantrell, T. Pellegrino, Magnetic nanoparticles and clusters for magnetic hyperthermia: optimizing their heat performance and developing combinatorial therapies to tackle cancer, *Chem. Soc. Rev.* 50 (2021) 11614–11667.
- [9] Y. Liu, P. Bhattarai, Z. Dai, X. Chen, Photothermal therapy and photoacoustic imaging via nanotheranostics in fighting cancer, *Chem. Soc. Rev.* 48 (2019) 2053–2108.
- [10] T.P. Ribeiro, J.A. Moreira, F.J. Monteiro, M.S. Laranjeira, Nanomaterials in cancer: reviewing the combination of hyperthermia and triggered chemotherapy, *J. Control Release* 347 (2022) 89–103.
- [11] M. Chang, Z. Hou, M. Wang, C. Li, J. Lin, Recent advances in hyperthermia therapy-based synergistic immunotherapy, *Adv. Mater.* 33 (2021), e2004788.
- [12] Q. Wu, N. Xia, D. Long, L. Tan, W. Rao, J. Yu, C. Fu, X. Ren, H. Li, L. Gou, P. Liang, J. Ren, L. Li, X. Meng, Dual-Functional supernanoparticles with microwave dynamic therapy and microwave thermal therapy, *Nano Lett.* 19 (2019) 5277–5286.
- [13] W.J. Zhi, L.F. Wang, X.J. Hu, Recent advances in the effects of microwave radiation on brains, *Military Medical Research* (4) (2017) 29.
- [14] L. Zhao, W. Zhang, Q. Wu, C. Fu, X. Ren, K. Lv, T. Ma, X. Chen, L. Tan, X. Meng, Lanthanide europium MOF nanocomposite as the theranostic nanoplatform for microwave thermo-chemotherapy and fluorescence imaging, *J. Nanobiotechnol.* 20 (2022) 133.
- [15] T. Li, Q. Wu, W. Wang, Z. Chen, L. Tan, J. Yu, C. Fu, X. Ren, P. Liang, J. Ren, L. Ma, X. Meng, MOF-derived nano-poppers synthesized by sonochemistry as efficient sensitizers for tumor microwave thermal therapy, *Biomaterials* (234) (2020), 119773.
- [16] J. Qi, W. Li, K. Lu, F. Jin, D. Liu, X. Xu, X. Wang, X. Kang, W. Wang, G. Shu, F. Han, X. Ying, J. You, J. Ji, Y. Du, pH and thermal dual-sensitive nanoparticle-mediated synergistic antitumor effect of immunotherapy and microwave thermotherapy, *Nano Lett.* 19 (2019) 4949–4959.
- [17] L. Wen, S. Yang, J. Zhong, Q. Zhou, D. Xing, Thermoacoustic imaging and therapy guidance based on ultra-short pulsed microwave pumped thermoelastic effect induced with superparamagnetic iron oxide nanoparticles, *Theranostics* (7) (2017) 1976–1989.
- [18] K.F. Chu, D.E. Dupuy, Thermal ablation of tumours: biological mechanisms and advances in therapy, *Nat. Rev. Cancer* 14 (2014) 199–208.
- [19] Q. Zhou, S. Shao, J. Wang, C. Xu, J. Xiang, Y. Piao, Z. Zhou, Q. Yu, J. Tang, X. Liu, Z. Gan, R. Mo, Z. Gu, Y. Shen, Enzyme-activatable polymer-drug conjugate augments tumour penetration and treatment efficacy, *Nat. Nanotechnol.* 14 (2019) 799–809.
- [20] Z. Ye, Y. Jiang, L. Li, F. Wu, R. Chen, Rational design of MOF-based materials for next-generation rechargeable batteries, *Nano-Micro Lett.* 13 (2021) 203.
- [21] R. Freund, O. Zaremba, G. Arnauts, R. Ameloot, G. Skorpurskii, M. Dincă, A. Bavykina, J. Gascon, A. Ejsmont, J. Goscińska, M. Kalmutzi, U. Lächelt, E. Ploetz, C.S. Diercks, S. Wuttke, The current status of MOF and COF applications, *Angew Chem. Int. Ed. Engl.* 60 (2021) 23975–24001.
- [22] D. Giliopoulos, A. Zamboulis, D. Giannakoudakis, D. Bikiaris, K. Triantafyllidis, Polymer/metal organic framework (MOF) nanocomposites for biomedical applications, *Molecules* (25) (2020).
- [23] S.S. Nadar, V.K. Rathod, Magnetic-metal organic framework (magnetic-MOF): a novel platform for enzyme immobilization and nanozyme applications, *Int. J. Biol. Macromol.* 120 (2018) 2293–2302.
- [24] X. Chen, R. Tong, Z. Shi, B. Yang, H. Liu, S. Ding, X. Wang, Q. Lei, J. Wu, W. Fang, MOF nanoparticles with encapsulated autophagy inhibitor in controlled drug delivery system for antitumor, *ACS Appl. Mater. Interfaces* 10 (2018) 2328–2337.
- [25] M.X. Wu, Y.W. Yang, Metal-organic framework (MOF)-Based drug/cargo delivery and cancer therapy, *Adv. Mater.* 29 (2017).
- [26] H.D. Lawson, S.P. Walton, C. Chan, Metal-organic frameworks for drug delivery: a design perspective, *ACS Appl. Mater. Interfaces* 13 (2021) 7004–7020.
- [27] H. Li, J. Sun, H. Zhu, H. Wu, H. Zhang, Z. Gu, K. Luo, Recent advances in development of dendritic polymer-based nanomedicines for cancer diagnosis, Wiley interdisciplinary reviews, *Nanomedicine and nanobiotechnology* 13 (2021), e1670.
- [28] A.G. Robertson, L.M. Rendina, Gadolinium theranostics for the diagnosis and treatment of cancer, *Chem. Soc. Rev.* 50 (2021) 4231–4244.
- [29] J. Wahsner, E.M. Gale, A. Rodríguez-Rodríguez, P. Caravan, Chemistry of MRI Contrast Agents: Current Challenges and New Frontiers, *Chemical reviews* (119) (2019) 957–1057.
- [30] R.H. Fang, W. Gao, L. Zhang, Targeting drugs to tumours using cell membrane-coated nanoparticles, *Nat. Rev. Clin. Oncol.* 20 (2023) 33–48.
- [31] J. Xia, Y. Xue, B. Lei, L. Xu, M. Sun, N. Li, H. Zhao, M. Wang, M. Luo, C. Zhang, B. Huang, Y. Du, C.H. Yan, Multimodal channel cancer chemotherapy by 2D functional gadolinium metal-organic framework, *Natl. Sci. Rev.* (8) (2021) nwa221.
- [32] X. Duan, C. Wang, J.C. Shaw, R. Cheng, Y. Chen, H. Li, X. Wu, Y. Tang, Q. Zhang, A. Pan, J. Jiang, R. Yu, Y. Huang, X. Duan, Lateral epitaxial growth of two-dimensional layered semiconductor heterojunctions, *Nat. Nanotechnol.* (9) (2014) 1024–1030.
- [33] Y. Chen, D. Ye, M. Wu, H. Chen, L. Zhang, J. Shi, L. Wang, Break-up of two-dimensional MnO<sub>2</sub> nanosheets promotes ultrasensitive pH-triggered theranostics of cancer, *Adv. Mater.* 26 (2014) 7019–7026.
- [34] G. Cheng, Z. Li, Y. Liu, R. Ma, X. Chen, W. Liu, Y. Song, Y. Zhang, G. Yu, Z. Wu, T. Chen, "Swiss Army Knife" black phosphorus-based nanodelivery platform for synergistic antiparkinsonian therapy via remodeling the brain microenvironment, *J. Control Release* 353 (2023) 752–766.
- [35] Z. Li, X. Lai, S. Fu, L. Ren, H. Cai, H. Zhang, Z. Gu, X. Ma, K. Luo, Immunogenic cell death activates the tumor immune microenvironment to boost the immunotherapy efficiency, *Adv. Sci.* 9 (2022), e2201734.
- [36] Y. Zhao, Y. Pan, K. Zou, Z. Lan, G. Cheng, Q. Mai, H. Cui, Q. Meng, T. Chen, L. Rao, L. Ma, G. Yu, Biomimetic manganese-based theranostic nanoplatform for cancer multimodal imaging and twofold immunotherapy, *Bioact. Mater.* 19 (2023) 237–250.
- [37] R.M. Chabanon, M. Rouanne, C.J. Lord, J.C. Soria, P. Pasero, S. Postel-Vinay, Targeting the DNA damage response in immuno-oncology: developments and opportunities, *Nat. Rev. Cancer* 21 (2021) 701–717.
- [38] G. Kroemer, C. Galassi, L. Zitvogel, L. Galluzzi, Immunogenic cell stress and death, *Nat. Immunol.* (23) (2022) 487–500.
- [39] Z. Li, H. Cai, Z. Li, L. Ren, X. Ma, H. Zhu, Q. Gong, H. Zhang, Z. Gu, K. Luo, A tumor cell membrane-coated self-amplified nanosystem as a nanovaccine to boost the therapeutic effect of anti-PD-L1 antibody, *Bioact. Mater.* 21 (2023) 299–312.
- [40] C. Chen, S. Zhao, A. Karnad, J.W. Freeman, The biology and role of CD44 in cancer progression: therapeutic implications, *J. Hematol. Oncol.* 11 (2018) 64.
- [41] E. Karousou, S. Misra, S. Ghatak, K. Dobra, M. Götte, D. Vignati, A. Passi, N. K. Karamanos, S.S. Skandalis, Roles and targeting of the HAS/hyaluronan/CD44 molecular system in cancer, *Matrix biology, journal of the International Society for Matrix Biology* 59 (2017) 3–22.
- [42] X. Xiao, H. Cai, Q. Huang, B. Wang, X. Wang, Q. Luo, Y. Li, H. Zhang, Q. Gong, X. Ma, Z. Gu, K. Luo, Polymeric dual-modal imaging nanoprobe with two-photon aggregation-induced emission for fluorescence imaging and gadolinium-chelation for magnetic resonance imaging, *Bioact. Mater.* 19 (2023) 538–549.
- [43] H. Jin, S. Qin, J. He, J. Xiao, Q. Li, Y. Mao, L. Zhao, New insights into checkpoint inhibitor immunotherapy and its combined therapies in hepatocellular carcinoma: from mechanisms to clinical trials, *Int. J. Biol. Sci.* 18 (2022) 2775–2794.
- [44] H.Z. Xu, T.F. Li, C. Wang, Y. Ma, Y. Liu, M.Y. Zheng, Z.J. Liu, J.B. Chen, K. Li, S. K. Sun, N. Komatsu, Y.H. Xu, L. Zhao, X. Chen, Synergy of nanodiamond-doxorubicin conjugates and PD-L1 blockade effectively turns tumor-associated macrophages against tumor cells, *J. Nanobiotechnol.* 19 (2021) 268.

- [45] A.H. Sharpe, K.E. Pauken, The diverse functions of the PD1 inhibitory pathway, *Nat. Rev. Immunol.* 18 (2018) 153–167.
- [46] T.Y. Seiwert, B. Burtness, R. Mehra, J. Weiss, R. Berger, J.P. Eder, K. Heath, T. McClanahan, J. Luceford, C. Gause, J.D. Cheng, L.Q. Chow, Safety and clinical activity of pembrolizumab for treatment of recurrent or metastatic squamous cell carcinoma of the head and neck (KEYNOTE-012): an open-label, multicentre, phase 1b trial, *Lancet Oncol.* 17 (2016) 956–965.
- [47] S. Jhunjhunwala, C. Hammer, L. Delamarre, Antigen presentation in cancer: insights into tumour immunogenicity and immune evasion, *Nat. Rev. Cancer* 21 (2021) 298–312.
- [48] F. Mami-Chouaib, C. Blanc, S. Cognac, S. Hans, I. Malenica, C. Granier, I. Tihy, E. Tartour, Resident memory T cells, critical components in tumor immunology, *J Immunother Cancer* (6) (2018) 87.
- [49] S. Healy, P. Khan, S. He, J.R. Davie, Histone H3 phosphorylation, immediate-early gene expression, and the nucleosomal response: a historical perspective, *Biochemistry and cell biology = Biochimie et biologie cellulaire* (90) (2012) 39–54.
- [50] Q. Wu, W. Wu, B. Fu, L. Shi, X. Wang, K. Kuca, JNK signaling in cancer cell survival, *Med. Res. Rev.* (39) (2019) 2082–2104.